Available online at www.sciencedirect.com
SCIENCE DIRECT®
ELSEVIER
International Journal of Solids and Structures 43 (2006) 4063–4081
INTERNATIONAL JOURNAL OF SOLIDS and STRUCTURES
www.elsevier.com/locate/ijsolstr

A theoretical investigation on the vibrational characteristics and torsional dynamic response of circumferentially cracked turbo-generator shafts

A. Vaziri [1], H. Nayeb-Hashemi *

Department of Mechanical, Industrial and Manufacturing Engineering, Northeastern University, 360 Huntington Ave., Boston, MA 02115, United States

Received 19 May 2005
Available online 15 July 2005

Abstract

Turbo-generator shafts are often subjected to complex dynamic torsional loadings, resulting in generation and propagation of circumferential cracks. Mode III fatigue crack growth generally results in a fracture surface consisting of peaks and valleys, resembling a factory roof. The fracture surface roughness depends on the material microstructure, the material yield strength, and the applied cyclic torque amplitude. This crack pattern can severely affect the vibration characteristics of the shafts. The accurate evaluation of the torsional dynamic response of the turbo-generator shafts entails considering the local sources of energy loss in the crack vicinity. The two most common sources of the energy loss are the local energy loss due to the plasticity at the crack tip and frictional energy loss due to interaction of mutual crack surfaces. A theoretical procedure for evaluating the values of the system loss factors corresponding to these sources of energy loss is presented. Furthermore, the local flexibility is obtained by evaluating the resistance of the cracked section of the shaft to the rotational displacement. The shaft material is assumed to be elastic perfectly plastic. The effects of the applied Mode III stress intensity factor and the crack surface pattern parameters on the energy loss due to the friction and the energy loss due to the plasticity at the crack tip are investigated. The results show that depending on the amplitude of the applied Mode III stress intensity factor, one of these energy losses may dominate the total energy loss in the circumferentially cracked shaft. The results further indicate that the torsional dynamic response of the turbo-generator shaft is significantly affected by considering these two sources of the local energy loss.

Keywords: Turbo-generator shafts; Circumferential crack; Transient torsional loading; Crack surface interaction; Crack tip plasticity; Torsional dynamic response; Local energy loss

* Corresponding author. Tel.: +1 617 373 5515; fax: +1 617 373 2921.
E-mail address: hamid@coe.neu.edu (H. Nayeb-Hashemi).
[1] Current address: Division of Engineering and Applied Sciences, Harvard University, Cambridge, MA 02138, USA.

0020-7683/$ - see front matter
doi:10.1016/j.ijsolstr.2005.05.029

Nomenclature

a	radius of uncracked region
a_i	dimensionless parameter
b	crack length
c_t	torsional damping constant
h	asperity height
k_t	torsional spring constant
r_P	plastic zone radius for Mode III cyclic loading
r^*	distance from the crack tip in a specified direction
x_1	extent of the crack surface interaction
u_1	axial crack opening displacement at the point x_1
$u_3(x)$	shear displacement
u_{3T}	shear displacement at the crack mouth
$\overline{uP}$	energy loss density at each point in the plastic zone
α	asperity angle
$\bar{\varepsilon}$	effective strain
$\bar{\sigma}$	effective stress
σ_0	normal stress at the crack tip, Case A
σ_Y	material yield stress
μ	columb friction coefficient
λ	asperity wavelength
ξ	dimensionless parameter
η	loss factor of the spring-damper model
η_P	loss factor of the model due to plasticity at the crack tip
η_f	loss factor of the model due to friction of the mating crack surfaces
ω	frequency of harmonic torque
Φ	response amplitude for the spring-damper model
Γ	effective frictional coefficient
E	material elastic modulus
G	material shear modulus
K_{eff}	effective stress intensity factor
K_{III}	applied stress intensity factor
K_{fric}	frictional stress intensity factor
L	shaft length
$M(\gamma)$	dimensionless parameter
$N_1(\gamma)$	dimensionless parameter
$N_2(\gamma)$	dimensionless parameter
R	shaft radius
R^*	extent of the plastic zone in a specified direction
T	applied torque
U_P	energy loss due to the plastic deformation at the crack tip in one cycle
U_f	energy loss due to friction between the mating fracture surfaces in one cycle
U	total energy loss in one cycle
ΔW	energy loss in one cycle for the spring-damper model

1. Introduction

The complex transient torsional loading history of turbo-generator shafts often results in initiation and propagation of circumferential cracks in these structural components, jeopardizing their structural integrity. To prevent the catastrophic failure of these shafts, a proper non-destructive evaluation method should be utilized in order to monitor its integrity during its service life. In recent years, the vibration-based inspection has been developed into an effective method for monitoring the structural integrity and detecting defects. This method is predominately based on monitoring the vibrational characteristics of the structural system and capturing their variation with the presence of defects (e.g. Vaziri and Nayeb-Hashemi, 2002, submitted for publication; Nayeb-Hashemi et al., 2003; Doebling et al., 1998; Dimarogonas, 1996; Krawczuk and Ostachowicz, 1996).

The accuracy of relating experimental data to the defect size and location depends on the analytical results that in turn depend on the proper modeling of cracked regions. The crack region is often modeled as a spring or an elastic hinge and the local energy loss on the crack region is ignored. This local energy loss contributes to the damping behavior of the system and could affect the dynamic behavior of the cracked structure significantly. The main sources of this energy loss are due to the plastic deformation at the crack tip and the friction between the mating fracture surfaces depending on the crack surface morphology and the load history. In a recent work, Vaziri and Nayeb-Hashemi (2002, submitted for publication) evaluated the local energy loss due to the plasticity at the crack tip of a viscoelastic-perfectly plastic bar with a penny shape crack subjected to a uniaxial harmonic loading. The energy loss due the plasticity at the crack tip was related to the plastic zone and the crack opening displacement. An equivalent viscous damping is exploited in the model in order to study the effect of local energy loss on the axial dynamic response of the bar. It was concluded that considering the local energy loss and material viscosity is essential for proper modeling of the dynamic response of the bar.

In contrast to Mode I crack growth, where there are little crack surfaces interactions, in Mode III, the mutual crack surfaces may interact in a complicated manner. The crack surface interactions occur when macroscopically rough crack faces are displaced relative to one another in shear, resulting in a contact pressure profile between the mutual crack surfaces. Readers are referred to Nayeb-Hashemi and McClintock (1982), Nayeb-Hashemi et al. (1983) for a detail discussion about the crack surface interactions in Mode III crack growth. In most of the pervious studies (e.g. Gasch, 1993; Sekhar and Prabhu, 1994) for evaluating the vibrational characteristics of cracked shafts, the effects of these crack surface interactions, as well as the energy loss due to the plasticity at the crack tip are ignored.

The objective of the present study is to evaluate the vibrational characteristics of turbo-generator shafts with a circumferential crack of various lengths by taking into account the local energy loss in the crack region due to the plasticity at the crack tip and the frictional energy loss due to the crack surface interactions.

2. Theoretical investigations

The schematic diagram of a shaft with a circumferential crack subjected to a dynamic torsional load, $T(t)$, is shown in Fig. 1. The shaft material is assumed linear elastic-perfectly plastic. In order to evaluate the torsional dynamic response of the shaft with a circumferential crack, a shaft model consisting of two segments connected by a torsional spring and a torsional damping is exploited, Fig. 2. The model torsional spring and the viscous torsional damper represent the local flexibility and the local energy loss of the crack region, respectively. The torsional spring constant is attained by evaluating the resistance of the crack section of the shaft to the rotational displacement. The model torsional damping constant is evaluated by considering the energy loss at the crack region due to the cyclic plasticity deformation at the crack tip and the frictional energy loss due to the crack surface interaction. The details of evaluating each of these model

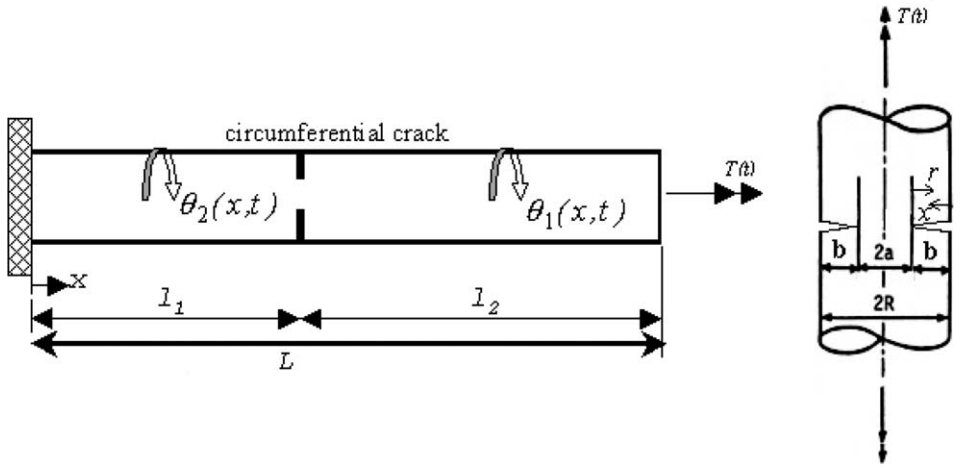

Fig. 1. Schematic model of a shaft with a circumferential crack.

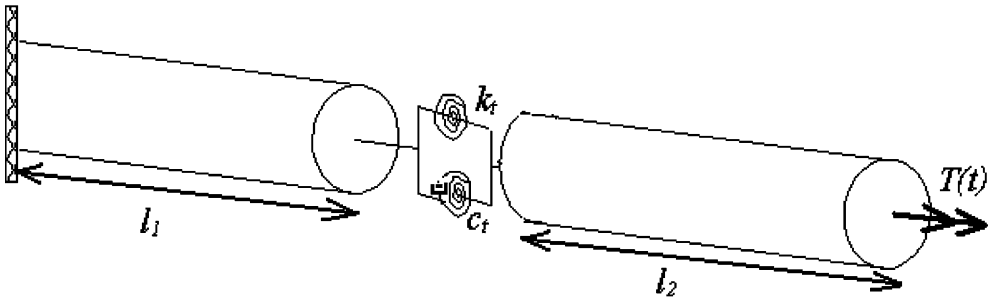

Fig. 2. The system model corresponding to Fig. 1.

components are described in Sections 2.1–2.3. In Section 2.4, the total loss factor of the model is related to the total energy loss per cycle in the shaft. Subsequently, the torsional dynamic response of a circumferentially cracked shaft model subjected to a harmonic torsional loading at its free end is evaluated in Section 2.5.

2.1. Torsional spring constant model

The torsional spring constant is related to the shear displacement at the crack mouth, u_{3T}, by

$$k_t = \frac{TR}{u_{3T}}, \tag{1}$$

where R is the shaft radius and T is the applied torque. The shear displacement along the crack is presented by Gross and Mendelsohn (1988) as,

$$u_3(x) = \frac{2K_{III}}{G\sqrt{\pi b}}(b^2 - x^2)^{0.5}, \tag{2}$$

where G is the shear modulus of the shaft material, b is the crack length and K_{III} is the applied Mode III stress intensity factor, which is obtained from (Tada et al., 2000),

$$K_{\mathrm{III}} = \frac{2T\sqrt{1-\gamma}}{\sqrt{\pi}R^{2.5}\gamma^{2.5}}\left[1+\frac{1}{2}\gamma+\frac{3}{8}\gamma^2+\frac{5}{16}\gamma^3+\frac{35}{128}\gamma^4+0.208\gamma^5\right], \tag{3}$$

where

$$\gamma = \frac{a}{R}, \tag{4}$$

where a is the radius of the uncracked region, Fig. 1. Eq. (3) is valid for $0 < \gamma < 1$. The model torsional spring constant can be evaluated by substituting (2) and (3) in (1) as,

$$k_{\mathrm{t}} = GR^3 M(\gamma), \tag{5}$$

where

$$M(\gamma) = \frac{\pi\gamma^{2.5}}{4(1-\gamma)\left[1+\frac{1}{2}\gamma+\frac{3}{8}\gamma^2+\frac{5}{16}\gamma^3+\frac{35}{128}\gamma^4+0.208\gamma^5\right]}. \tag{6}$$

Fig. 3 shows the variation of dimensionless parameter, $M(\gamma)$ with γ.

2.2. Evaluating the energy loss due to cyclic plasticity at the crack tip

The energy loss due to the plastic deformation at the crack tip is obtained by assuming the plastic zone size as a circle at the crack tip with the radius, r_{P}, Fig. 4. The radius of the plastic zone for Mode III cyclic loading can be estimated from (Broek, 1978),

$$r_{\mathrm{P}} = \frac{3}{2\pi}\left(\frac{K_{\mathrm{eff}}}{\sigma_{\mathrm{Y}}}\right)^2. \tag{7}$$

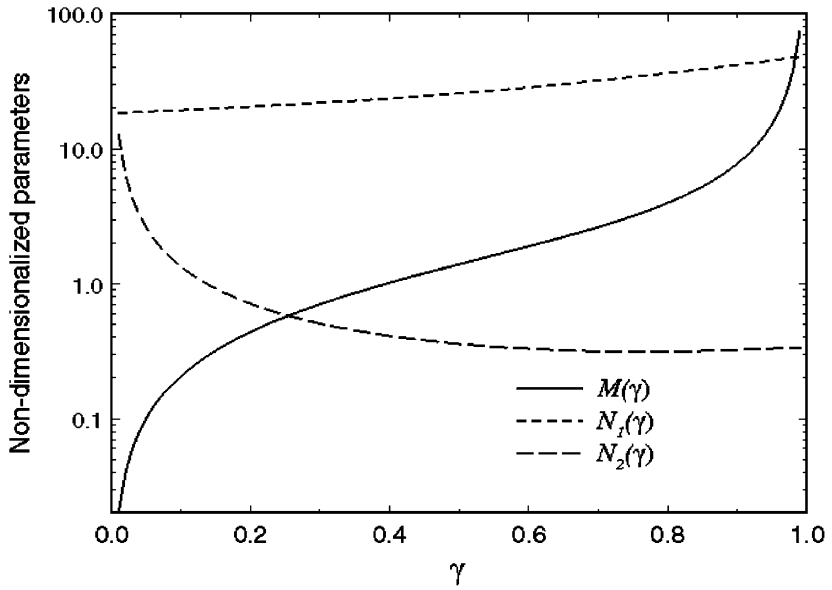

Fig. 3. Variation of non-dimensionalized parameters used in the theoretical investigation vs. γ.

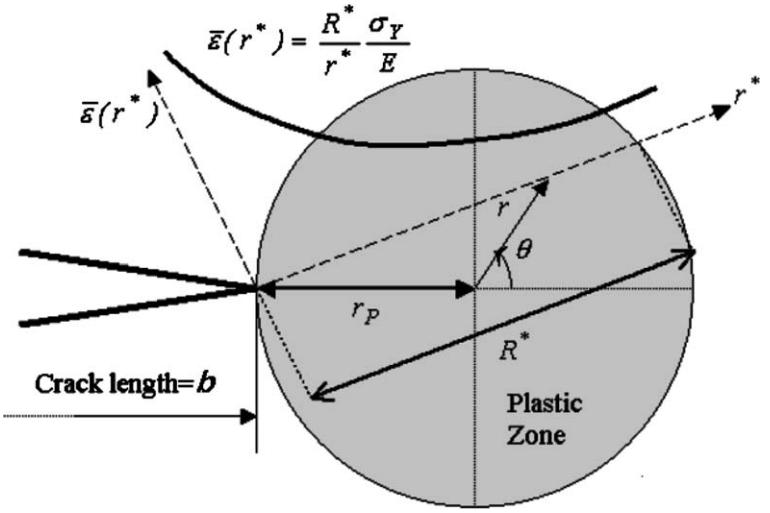

Fig. 4. Variation of the effective strain in a particular direction inside the plastic zone.

The energy loss density due to the plastic deformation at any point in the plastic zone at the crack tip can be approximated as (Chen and Han, 1988),

$$\bar{u}_P(r,\theta) = \bar{\sigma}\bar{\varepsilon}, \tag{8}$$

where $\bar{u}_P$ is the energy density, $\bar{\sigma}$ and $\bar{\varepsilon}$ are the effective stress and strain, respectively. Because the material is elastic-perfectly plastic, $\bar{\sigma}$ is equal to the yield stress of the material, σ_Y. The effective strain, $\bar{\varepsilon}$ at the edge of the plastic zone is taken as σ_Y/E, where E is the shaft material Young's modulus. The effective plastic strain inside the plastic zone can be approximated as (Nayeb-Hashemi and Taslim, 1987),

$$\bar{\varepsilon}(r,\theta) = \frac{R^*}{r^*}\frac{\sigma_Y}{E}, \tag{9}$$

where r^* and R^* are the distance from the crack tip and the extent of the plastic zone in a particular direction, (r,θ), Fig. 4. By substituting (9) in (8), the energy loss density at each point in the plastic zone can be presented as,

$$\overline{u_P}(r,\theta) = \frac{R^*}{r^*}\frac{\sigma_Y^2}{E}. \tag{10}$$

Then, the total energy loss due to the plastic deformation at the crack tip in half cycle can be evaluated by integrating the energy loss density over the plastic zone volume,

$$U_P = \left(\int_{\theta=0}^{2\pi}\int_{r=0}^{r_P}\frac{R^*}{r^*}\frac{\sigma_Y^2}{E}r\,d\theta\,dr\right)2\pi a \tag{11}$$

this results in,

$$U_P = \frac{4\pi^2 a r_P^2 \sigma_Y^2}{E}. \tag{12}$$

This equation presents an approximation for the energy loss due to cyclic plasticity for half cycle of harmonic oscillation for the elastic-perfectly plastic turbo-generator shaft with the circumferential crack of length a.

2.3. Energy loss due to frictional energy loss between the mutual crack surfaces

The frictional energy loss in one cycle for a specified turbo-generator shaft with a certain circumferential crack length due to harmonic torsional oscillation depends on the crack surface interaction length and the pressure profile arising along the interaction zone. This is a complex function of crack surface morphology and the applied Mode III stress intensity factor. The frictional energy loss in one cycle due to friction between the mating fracture surfaces can be presented as,

$$U_{\mathrm{f}} = 2\pi \int_0^{2\pi/\omega} \int_0^b (R-x)\sigma_R(x,t)\dot{u}_{3,\mathrm{eff}}(x,t)\,\mathrm{d}x\,\mathrm{d}t, \tag{13}$$

where $\sigma_R(x,t)$ is the frictional stress profile between cracked surfaces at any point and ω is the frequency of applied torque. $\dot{u}_{3,\mathrm{eff}}(x,t)$ is the relative velocity of the crack surfaces under dynamic torsional loading. The relative velocity of the crack surfaces under torsional loading can be obtained from the Mode III shear displacement,

$$u_{3,\mathrm{eff}}(x,t) = \frac{2K_{\mathrm{eff}}(t)}{G\sqrt{\pi b}}\left(b^2-x^2\right)^{0.5}. \tag{14}$$

The effective Mode III stress intensity factor is related to the applied Mode III stress intensity factor, $K_{\mathrm{III}}(t)$, and the frictional stress intensity factor arises due to the interactions of the crack surfaces, $K_{\mathrm{fric}}(t)$, by

$$K_{\mathrm{eff}}(t) = K_{\mathrm{III}}(t) - K_{\mathrm{fric}}(t). \tag{15}$$

The frictional Mode III stress intensity factor is presented by Gross and Mendelsohn (1989) as,

$$K_{\mathrm{fric}}(t) = -\left(\frac{b}{\pi}\right)^{0.5} \int_0^b \frac{\sigma_R(x,t)}{\left(b^2-x^2\right)^{0.5}}\,\mathrm{d}x. \tag{16}$$

The frictional stress profile between the mutual crack surfaces and the interaction zone can be evaluated by exploiting the crack pattern. Fig. 5 shows a typical fracture surface pattern of a shaft with a circumferential crack and its interaction due to cyclic torque with various amplitudes. The reader is referred to Nayeb-Hashemi and McClintock (1982) and Nayeb-Hashemi et al. (1983) for details about the experiments and the discussion about initiation and propagation of the circumferential crack in turbo-generator shafts under cycling torsional loading. At high cyclic Mode III stress intensity factor, the circumferential crack growth results in a macroscopically flat fracture surface. However, at low cyclic Mode III stress intensity factor circumferential crack growth results in a rough fracture surface, which resembles a factory roof. The fracture surface roughness depends on the material microstructure, the material yield strength, and the applied cyclic torque amplitude. This crack pattern results in interaction between mutual crack surfaces, which results in the frictional energy loss. Here, we consider the fracture surface as consisting of peaks and valleys with average roughness height h, and an average wavelength λ, see Fig. 6. This assumption is somewhat in agreement with the experimental results from Nayeb-Hashemi et al. (1983) and Nayeb-Hashemi and McClintock (1982). Then, the frictional stress can be related to the normal contact stress, $\sigma_{\mathrm{c}}(x,t)$, by,

$$\sigma_R(x,t) = \Gamma\sigma_{\mathrm{c}}(x,t), \tag{17}$$

where Γ is the effective frictional coefficient that can be related to coulomb friction coefficient, μ, and asperity angle, α,

$$\Gamma = \frac{\tan\alpha + \mu}{1 - \mu\tan\alpha}. \tag{18}$$

Fig. 5. Circumferential crack propagation patterns for a shaft under various applied torques.

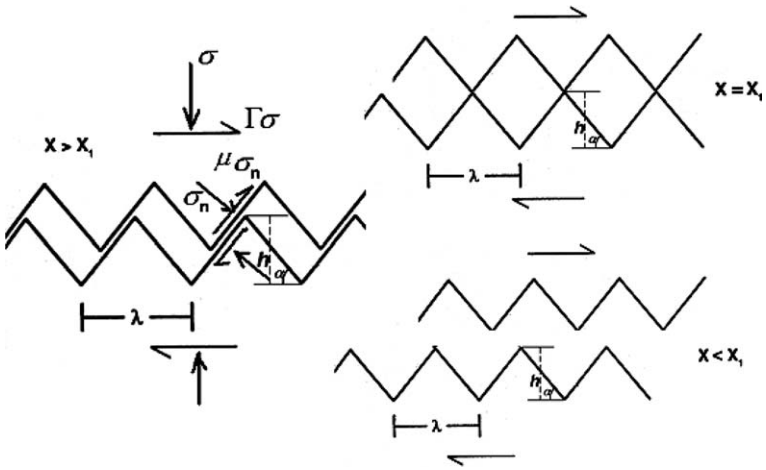

Fig. 6. The crack pattern which consists of peak and valleys with an average amplitude of roughness, h, and an average wavelength, λ, presenting the factory roof crack surface morphology. At $x = x_1$, the shear displacement of the crack surface is equal to half wavelength of the asperities, $\lambda/2$ and the crack opening displacement is equal to the asperity height h. For $x > x_1$, where the shear displacement of the crack tip is greater than half wavelength of the asperities, no interaction is assumed between the mutual crack surfaces. For $x < x_1$, the interaction between the mutual crack surfaces generates stress profile normal and parallel to the crack surface.

Here the asperity angle can be related to the average asperities height and its wavelength, $\alpha = \arctan(2h/\lambda)$, Fig. 6.

Substituting (16) and (17) in Eq. (13), the frictional energy loss in one cycle for the circumferentially cracked turbo-generator shaft exhibiting the crack surface pattern depicted in Fig. 6, can be represented as,

$$U_f = \frac{4\sqrt{\pi}\Gamma}{G\sqrt{b}} \int_0^{2\pi/\omega} \int_0^b (R-x)(b^2-x^2)^{0.5}\sigma_c(x,t)\frac{\partial K_{eff}(t)}{\partial t}\,dx\,dt. \tag{19}$$

In order to calculate the frictional energy loss, the normal contact pressure profile and the effective Mode III stress intensity factor should be evaluated, which are complex functions of the crack pattern parameters, coefficient of friction between the crack surfaces and applied Mode III stress intensity factor. Vaziri and Nayeb-Hashemi (2003, 2005) developed a theoretical procedure to evaluate the normal pressure profile along the crack and the effective Mode III stress intensity factor. These could be obtained by considering that the Mode III shear displacement at the extent of the interaction, x_1 is equal to asperities half wavelength, $\lambda/2$ (λ is the average wavelength, Fig. 6) and the crack opening displacement at this point is equal to the asperities height, h. Three possible pressure profiles due to the crack surfaces interaction are assumed, Fig. 7, in order to evaluate the effective Mode III stress intensity factor under various applied Mode III stress intensity factors. For all of these cases, the extent of the crack surface interaction, x_1, can be evaluated by equating the Mode III shear displacement from (14), to the half wavelength,

$$x_1 = b\sqrt{1-\frac{\pi G^2\lambda^2}{16K_{eff}^2}}. \tag{20}$$

It is assumed that there is no interaction between the crack surfaces for $x < x_1$. This assumption can be justified by considering that the Mode I displacement is greater than the asperity average height for $x < x_1$. The frictional energy loss for each pressure profile of Fig. 7 and the procedure for defining the normal pressure profile parameters are presented in Appendix A. Readers are referred to Vaziri and Nayeb-Hashemi (2005) for details concerning the theoretical investigation.

2.4. Total loss factor of the system

The total energy loss per cycle in the turbo-generator shaft is related to the energy loss due to cyclic plasticity at the crack tip and the fictional energy loss due to the crack surface interaction,

$$U = 2U_P + U_f. \tag{21}$$

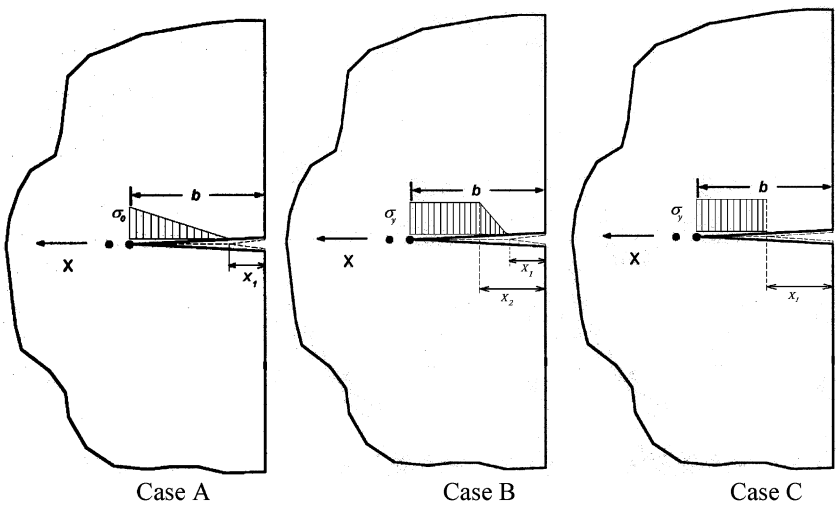

Fig. 7. Possible pressure distribution profiles between mating fracture surfaces arising from the crack surface interactions.

In addition, the energy loss per cycle in the model, Fig. 2, subjected to the torsional oscillation at the frequency of ω and amplitude Φ can be presented as (Rao, 2004),

$$\Delta W = \pi \Phi^2 \omega c_t, \tag{22}$$

where c_t is the model torsional damping constant. The amplitude of the response can be related to the shear displacement at the crack mouth, $u_{3T,eff}$,

$$\Phi = \frac{u_{3T,eff}}{R}. \tag{23}$$

The shear displacement at the crack mouth, $u_{3T,eff}$, is evaluated from (13),

$$u_{3T,eff} = \frac{2K_{eff}\sqrt{b}}{G\sqrt{\pi}}. \tag{24}$$

The torsional damping constant is attained by equating the total energy loss per cycle in the model from (22) to the total energy loss per cycle in the shaft due to the cyclic plasticity at the crack tip and the frictional energy loss, Eq. (21) as,

$$c_t = \frac{8\pi a r_P^2 \sigma_Y^2 R^2}{E u_{3T,eff}^2 \omega} + \frac{U_f R^2}{\pi u_{3T,eff}^2 \omega}. \tag{25}$$

Substituting (7) and (24) in (25) results in,

$$c_t = \frac{72 K_{eff}^2 a R^2 G^2}{E \omega b \sigma_Y^2} + \frac{U_f R^2 G^2}{4 K_{eff}^2 \omega b}. \tag{26}$$

The local flexibility and damping of the model can be combined by utilizing a complex stiffness, k_t^*,

$$k_t^* = k_t(1 + i\eta), \tag{27}$$

where k_t is the torsional stiffness from (5) and $\eta = c_t\omega/k_t$ is the system loss factor, which can be presented in terms of the loss factors due to the plasticity at the crack tip, η_P, and due to the friction of the mating crack surfaces, η_f, as,

$$\eta = \eta_P + \eta_f, \tag{28}$$

where

$$\eta_P = \frac{K_{eff}^2}{(1+\nu) R \sigma_Y^2} N_1(\gamma) \tag{29}$$

$$\eta_f = \frac{U_f G}{K_{eff}^2 R^2} N_2(\gamma) \tag{30}$$

and

$$N_1(\gamma) = \frac{36\gamma}{(1-\gamma) M(\gamma)} \tag{31}$$

$$N_2(\gamma) = \frac{1}{4(1-\gamma) M(\gamma)} \tag{32}$$

The variations of the dimensionless parameters $N_1(\gamma)$ and $N_2(\gamma)$ with γ are presented in Fig. 3.

2.5. Torsional dynamic response of the system

The torsional dynamic response of the turbo-generator shaft subjected to a harmonic torsional loading at its free end, $T_0 e^{i\omega t}$, is evaluated considering the equations of motion for each segment shown in Fig. 2 and their corresponding boundary conditions. The displacement function $\theta_i(x,t)$, corresponding to each of the model segments when the shaft is subjected to harmonic torsional loading is of the type,

$$\theta_i(x,t) = \overline{\theta_i}(x)e^{i\omega t} \quad \text{where } i = 1 \text{ and } 2 \tag{33}$$

by introducing the following dimensionless parameters,

$$a_i = \frac{\rho_i L^2 \omega^2}{G_i} \quad \text{where } i = 1 \text{ and } 2 \tag{34}$$

$$\xi = \frac{x}{L} \tag{35}$$

The governing equation of rotational motion for each segment of Fig. 2, in the front and back of the crack faces, is presented by,

$$\frac{d^2\overline{\theta_i}(x)}{d\xi^2} + a_i\overline{\theta_i}(x) = 0 \quad \text{where } i = 1 \text{ and } 2. \tag{36}$$

Solution of (36) is in the form of:

$$\overline{\theta_i}(x) = \sum_{j=1}^{2} A_{ij} e^{S_{ij}\zeta}, \tag{37}$$

where $S_{i1} = i\sqrt{a_i}$, and $S_{i2} = -i\sqrt{a_i}$ $(i = -\sqrt{1})$ and A_{ij}s are constants which can be calculated from the boundary conditions of each segment.

3. Results and discussions

The results are provided for 4140 steel (in annealed condition) shaft of 0.4 m long and 0.1 m radius with a circumferential crack. Table 1 shows the mechanical properties of 4140 steel. It is assumed that the material properties are not sensitive to strain rate. All the results presented here are for constant radius of the shaft, $R = 10$ cm, and constant crack length equal to half of the shaft radius, $\gamma = 0.5$. Furthermore, the coefficient of friction between the mating surfaces is assumed to be constant, $\mu = 0.75$. The applied torsion to the shaft is harmonic. Based on the theoretical investigations presented in Section 2.3, a set of MATLAB and MAPLE codes are developed to calculate the effective Mode III stress intensity factor and normal pressure distribution along the crack. The frictional energy loss per cycle is obtained by numerically evaluating the right hand side of Eq. (13).

Table 1
Material properties of the shafts

Material	4140 steel, in annealed condition
Density	7850 kg/m^3
Poisson's ratio	0.3
Elastic modulus	200 GPa
Yield stress	420 MPa

3.1. Vibrational characteristics of the circumferentially cracked shaft

Fig. 8 presents the effective Mode III stress intensity factor for various Mode III stress intensity factor applied to the shaft with fracture surface roughness $\lambda = 100$ μm, $h = 10$ μm. The results indicate that a critical value for the applied Mode III stress intensity factor can be identified (critical theoretical SIF = 61.5 MPa$\sqrt{m}$), which results in a little crack surface interaction and sudden burst in the Mode III crack sliding. Furthermore, the results show that the value of this critical theoretical SIF, exhibits a very low sensitivity to the crack length and mainly depends on the crack surface morphology (asperities height and wavelength). Vaziri and Nayeb-Hashemi (2003, 2005) have investigated the effect of these parameters on this critical value.

The variation of the frictional energy loss in one cycle due to friction between the mating fracture surfaces with the amplitude of applied Mode III stress intensity factor is depicted in Fig. 8. The results show that the frictional energy loss increases with increasing the amplitude of applied Mode III stress intensity factor. The frictional energy loss exhibits a very little sensitivity to the amplitude of Mode III stress intensity factor for the applied Mode III stress intensity factor greater than the critical value. This could be justified considering the very small region of interaction between the mating fracture surfaces for the applied stress intensity factor greater than the critical value.

Fig. 9 shows the variation of the loss factors due to the plasticity at the crack tip and frictional energy loss vs. the amplitude of applied Mode III stress intensity factor. The results indicate that for the amplitude of applied Mode III stress intensity factor lower than the critical value, the energy loss due to the friction dominates the energy loss characteristics of the system. However, for the applied Mode III stress intensity factor greater than the critical value, the energy loss due to the plasticity at the crack tip dominates the energy loss in the system. While the frictional energy loss per cycle is almost constant for the amplitude of applied Mode III stress intensity factor equal or greater than the critical value (Fig. 8). The potential energy stored in the elastic part of the model (torsional spring) increases significantly at the critical value of the applied Mode III stress intensity factor. This results in reduction of the frictional loss factor (the loss factor is defined as the energy loss in a cycle to the maximum potential energy stored in the model). In contrast,

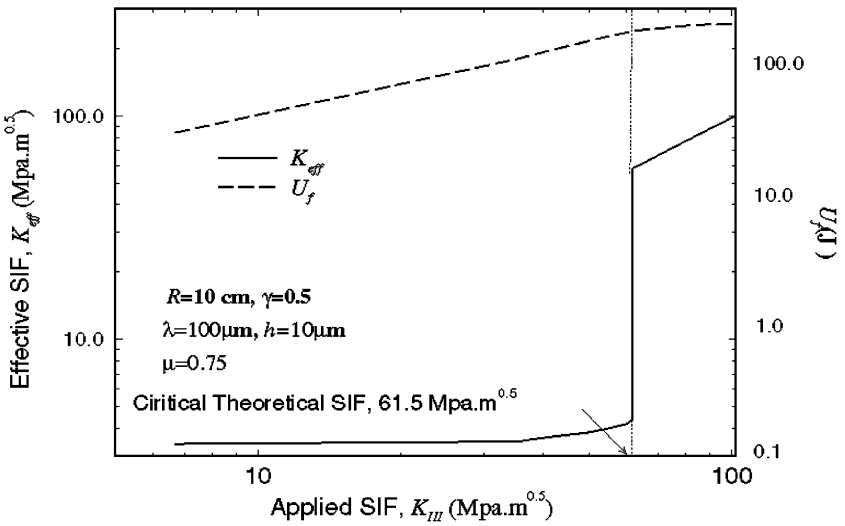

Fig. 8. Variation of the effective stress intensity factor, K_{eff} and the frictional energy loss in a cycle, U_{f} vs. the applied stress intensity factor, K_{III}.

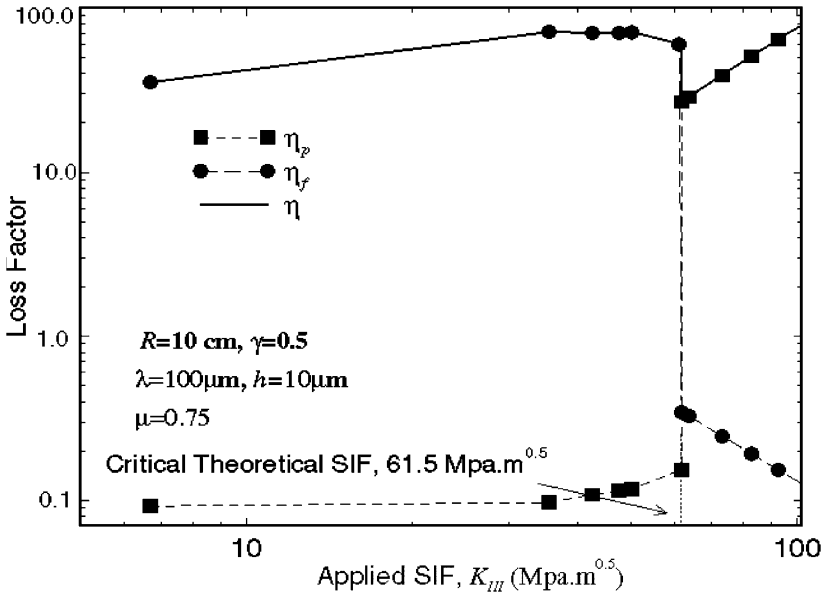

Fig. 9. Variation of the loss factors of the model vs. the applied stress intensity factor, K_{III}.

since the plastic zone is a function of the effective stress intensity factor, the energy loss due to cyclic plasticity at the crack tip increases abruptly at the critical value of the applied Mode III stress intensity factor. The total loss factor of the system is minimized at the critical applied Mode III stress intensity factor.

The model loss factors and its components (due to frictional and due to plasticity) are functions of the crack surface morphology. Here, limited results are provided depicting the effect of the average asperities height on the variation of each of these loss factors with the amplitude of Mode III stress intensity factor (Figs. 10–12). The total loss factor and its components exhibit a drastic change as the applied stress intensity factor approaches the critical stress intensity factor. This drastic change in the components of the total loss factor is more pronounced for rougher fracture surfaces (higher asperities height). Furthermore, the results indicate that the frictional loss factor is more sensitive to the crack surface morphology (represented here with two parameters, λ and h). The total loss factor of the system exhibits significantly lower sensitivity to the crack surface morphology than its components.

3.2. Torsional dynamic response of the circumferentially cracked shaft

Fig. 13 shows the frequency response of the shaft at the point of applied load under a harmonic torsional load with the amplitude of 1 N m, for various local energy loss factors, η. The circumferential crack is located at the middle of the shaft with the crack size of $\gamma = 0.5$. The results indicate that the local energy loss affects the amplitude of the vibration, as well as the frequencies where peak responses occur. The amplitude of the system drastically reduces with the introduction of the local loss factor into the system response. However, further increase in the local loss factor, apparently increases the amplitude of the system response. This can be justified considering that the system response depends on the energy loss and stiffness of the cracked section.

A dimensionless parameter, $\psi(n)$, is defined as the ratio of the nth peak response frequency of the circumferentially cracked shaft to the nth resonant frequency of the perfect shaft (without crack). The

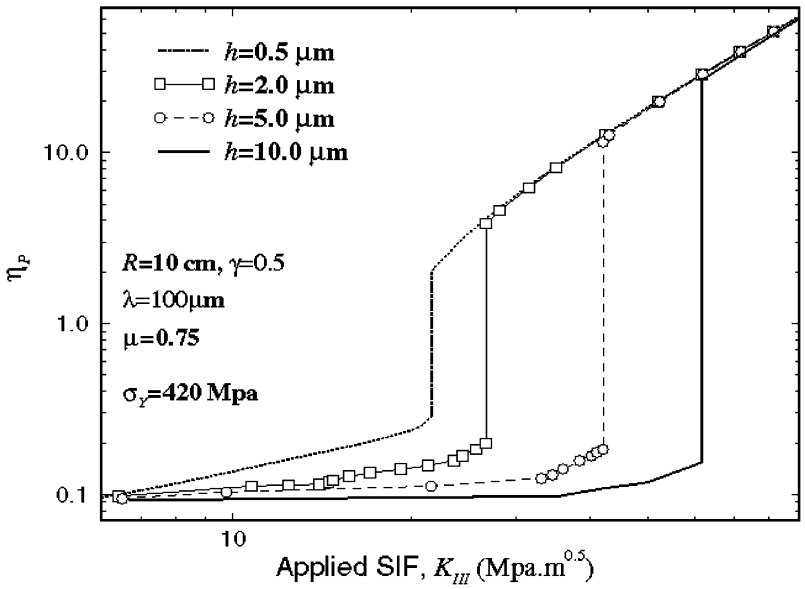

Fig. 10. Variation of the loss factor due to the plasticity at the crack tip, η_P vs. the applied Mode III stress intensity factor, K_{III}, for various average asperities heights.

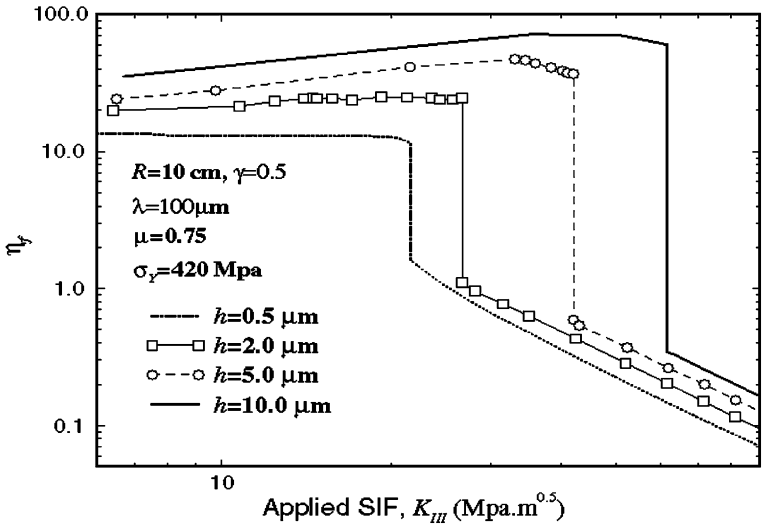

Fig. 11. Variation of the loss factor due to the friction of the mating fracture surfaces, η_f vs. the applied Mode III stress intensity factor, K_{III} for various average asperities heights.

variation of the first three dimensionless peak response frequencies of the circumferentially cracked shaft, $\psi(n)$, $n = 1$–3, with the local energy loss, η, is shown in Fig. 14.

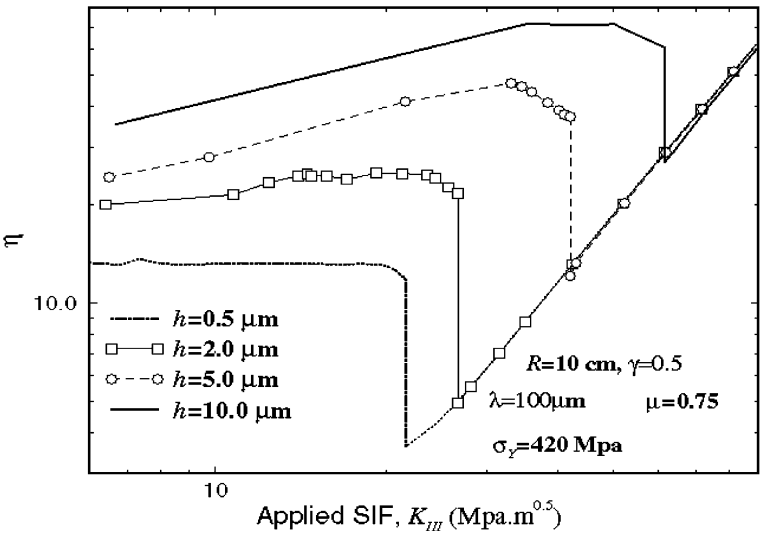

Fig. 12. Variation of the system total loss factor, η vs. the applied Mode III stress intensity factor, K_{III} for various average asperities heights.

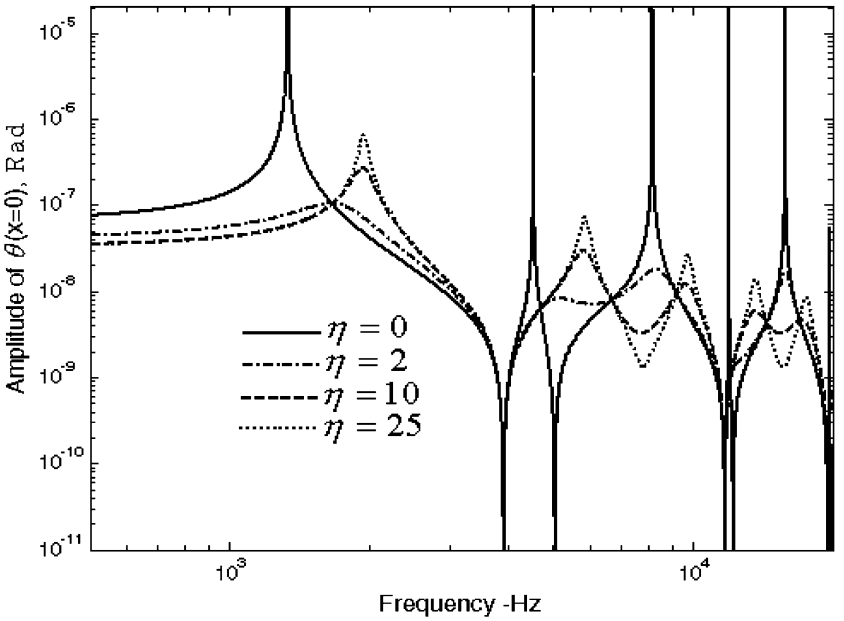

Fig. 13. Effects of the local energy loss on the frequency response of the shaft with a circumferential crack, $\gamma = 0.5$ for a crack located at the middle of the bar, $l_1 = l_2$.

The results show that the peak response frequencies of the system initially increase drastically with increasing the local loss factor, approaching the resonant frequencies of the uncracked shafts. However, beyond a critical loss factor, the system peak response frequencies exhibit a very small sensitivity to the

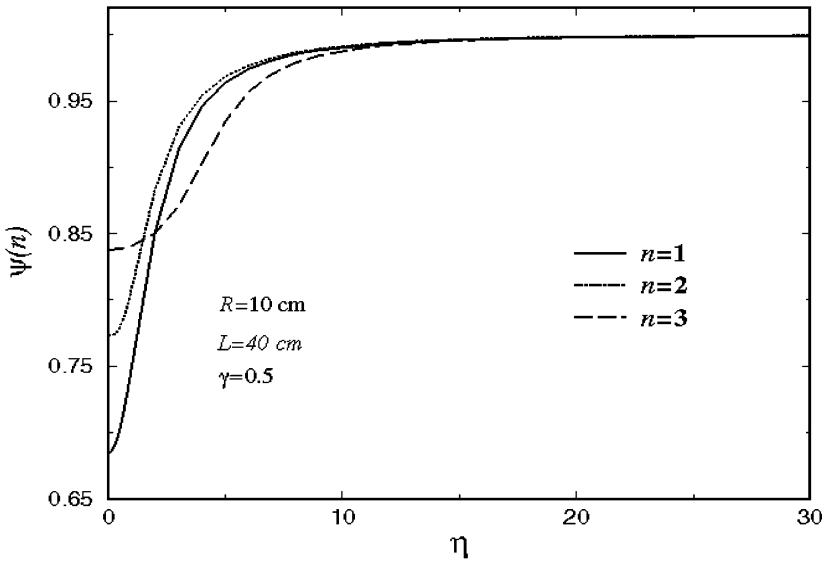

Fig. 14. Variations of the first–third non-dimensionalized peak response frequencies of the shaft with a circumferential crack, $\gamma = 0.5$ vs. the local loss factor, for a cracked located at the middle of the bar, $l_1 = l_2$.

local loss factor. The sensitivity of the peak response frequency to the local loss factor is more pronounced for lower peak response frequencies for the geometry and crack location studied.

4. Concluding remarks

A theoretical procedure is developed to evaluate the energy loss in a shaft with a circumferential crack and macroscopically rough fracture surface, subjected to cyclic torsion. The energy loss stems from the cyclic plasticity at the crack tip and frictional energy loss due to fracture surface interactions. The results are obtained for a wide range of applied cyclic Mode III stress intensity factor amplitude and for a specified crack length and fracture surface morphologies. The results of the analysis indicate that for a specified crack length and fracture surface morphology; there exists a critical value of amplitude of applied Mode III stress intensity factor where crack surface interactions diminish. For the applied Mode III stress intensity factor of less than the critical value, the dominant mechanism of energy loss is due to friction between the fracture surfaces. In contrast, for the amplitude of applied stress intensity factor greater than this critical value, the energy loss due to plasticity at the crack tip is the dominant mechanism of energy loss as the frictional energy loss becomes negligible. The value of this critical stress intensity factor depends on the fracture surface morphology (asperities height and wavelength). The effect of fracture surface crack pattern parameters on the variation of the shaft energy losses with the amplitude of applied Mode III stress intensity factor is presented. The loss factors due to the friction between the mutual crack surfaces and cyclic plasticity at the crack tip are defined based on their contribution in the energy loss of the system in one cycle. Apparently, the loss factor due to friction between the mutual crack surfaces exhibits higher sensitivity to the crack pattern parameters (fracture surface asperities height and wavelength).

The torsional dynamic response of the circumferentially cracked shaft is evaluated by taking into account the effect of the local energy loss. The results indicate that the local energy loss affects the amplitude of the vibration, as well as the peak response frequencies of the cracked shaft. The results show that by increasing the local loss factor the peak response frequencies of the cracked shaft approaches to the reso-

nant frequencies of the uncracked shaft. However, further increase of the system loss factor does not affect the peak response frequencies of the system. It can be concluded that monitoring the peak response frequencies and amplitude of the response as a vibration-based non-destructive technique may result in an inaccurate conclusion regarding the presence of a crack in a turbo-generator shaft. However, monitoring the damping of the cracked shaft, in addition to the peak response frequencies and amplitude may provide enough information for crack detection. Panteliou et al. (2001) and Panteliou and Dimarogonas (1997) evaluated the damping behavior of a homogeneous, isotropic, elasto-plastic bar with a single-edge crack under alternating uniform axial stress considering the non-reversible heat flow from areas of higher heat generation to the lower heat generation. They suggested that the local damping could be exploited as a vibration parameter to predict the crack severity and its location.

Appendix A

The normal pressure profile parameters are attained by simultaneously satisfying the Mode I crack opening displacement and Mode III crack displacement at the point x_1. This requires solution of a set of non-linear equations. It should be noted that if the applied torque is very small, the pressure distribution parameters might not be obtainable by exploiting this theoretical procedures. This may suggest that the Mode III crack mouth displacement is less than half of the asperities wavelength. In this case, an experimental data regarding Mode III crack mouth displacement is required, in order to obtain the pressure profile parameters.

The assumed pressure profile and the corresponding frictional Mode III stress intensity factor for each stress distribution of Fig. 7 are as follows.

Case A. The normal stress varies linearly from the maximum value of $\sigma_0 \leqslant \sigma_Y$ at the crack tip to zero at x_1,

$$\sigma(x) = \begin{cases} 0, & 0 < x < x_1, \\ \sigma_0 \dfrac{x - x_1}{b - x_1}, & x_1 < x < b, \end{cases} \tag{A.1}$$

where the maximum value of stress, σ_0

$$\sigma_0 = -\frac{h\pi E}{8\chi_1(R, b, x_1)} \tag{A.2}$$

and

$$\chi_1(R, b, x_1) = \left[\int_{x_1}^{b} (R - x)(x - x_1)\,\mathrm{d}x \int_{x}^{b} \frac{1}{(R - b)^2 (b - x_1)} \left\{ \cos^{-1} \frac{R - b}{R - x_1} + \frac{R - b}{\sqrt{(R - x_1)^2 - (R - b)^2}} \right\} \right.$$
$$\left. \times \left\{ \cos^{-1} \frac{R - b}{R - x} + \frac{R - b}{\sqrt{(R - x)^2 - (R - b)^2}} \right\} \mathrm{d}b \right]. \tag{A.3}$$

The frictional Mode III stress intensity factor for this pressure profile can be obtained by substituting (17), (18), (A.1) and (A.2) in (16),

$$K_{\mathrm{fric}} = \left(\frac{b}{\pi} \right)^{0.5} \frac{h\pi E \Gamma}{8\chi(R, b, x_1)(b - x_1)} \int_{x_1}^{b} \frac{(x - x_1)}{(b^2 - x^2)^{0.5}}\,\mathrm{d}x. \tag{A.4}$$

Case B. The normal stress is equal to the material yield stress from the crack tip to a point at the distance x_2 from the crack tip, then decreases linearly to the extent of interaction point, x_1,

$$\sigma(x) = \begin{cases} 0, & 0 < x < x_1, \\ \sigma_Y \dfrac{x - x_1}{x_2 - x_1}, & x_1 < x < x_2, \\ \sigma_Y, & x_2 < x < b, \end{cases} \tag{A.5}$$

where x_2 can be obtained from $u_1(x_1) = h$, which results in,

$$h = -\frac{8\sigma_Y}{\pi E'} \chi_2(R, b, x_1, x_2), \tag{A.6}$$

where

$$\begin{aligned} \chi_2(R, b, x_1, x_2) = & \left\{ \int_{x_2}^{b} (R - x)\, \mathrm{d}x \int_{x}^{b} \frac{1}{(R-b)^2} \left\{ \cos^{-1} \frac{R-b}{R-x_1} + \frac{R-b}{\sqrt{(R-x_1)^2 - (R-b)^2}} \right\} \right. \\ & \left. \times \left\{ \cos^{-1} \frac{R-b}{R-x} + \frac{R-b}{\sqrt{(R-x)^2 - (R-b)^2}} \right\} \mathrm{d}b \right. \\ & + \int_{x_1}^{x_2} (R - x)(x - x_1)\, \mathrm{d}x \int_{x}^{b} \frac{1}{(R-b)^2 (x_2 - x_1)} \left\{ \cos^{-1} \frac{R-b}{R-x_1} + \frac{R-b}{\sqrt{(R-x_1)^2 - (R-b)^2}} \right\} \\ & \left. \times \left\{ \cos^{-1} \frac{R-b}{R-x} + \frac{R-b}{\sqrt{(R-x)^2 - (R-b)^2}} \right\} \mathrm{d}b \right\}. \end{aligned} \tag{A.7}$$

The frictional Mode III stress intensity factor can be calculated from,

$$K_{\mathrm{fric}} = -\left(\frac{b}{\pi}\right)^{0.5} \Gamma \sigma_Y \left[\frac{1}{x_2 - x_1} \int_{x_1}^{x_2} \frac{x - x_1}{(b^2 - x^2)^{0.5}}\, \mathrm{d}x + \int_{x_2}^{b} \frac{1}{(b^2 - x^2)^{0.5}}\, \mathrm{d}x \right]. \tag{A.8}$$

Case C. The normal stress is equal to the yield stress of the material along the interaction zone,

$$\sigma(x) = \begin{cases} 0, & 0 < x < x_1, \\ \sigma_Y, & x_1 < x < b. \end{cases} \tag{A.9}$$

The frictional Mode III stress intensity factor for this case is,

$$K_{\mathrm{fric}} = -\left(\frac{b}{\pi}\right)^{0.5} \Gamma \sigma_Y \left[\frac{1}{x_2 - x_1} \int_{x_1}^{x_2} \frac{x - x_1}{(b^2 - x^2)^{0.5}}\, \mathrm{d}x + \int_{x_2}^{b} \frac{1}{(b^2 - x^2)^{0.5}}\, \mathrm{d}x \right]. \tag{A.10}$$

References

Broek, D., 1978. Elementary Engineering Fracture Mechanics. Sijthoff & Noordhoff.

Chen, W.F., Han, D.J., 1988. Plasticity for Structural Engineers. Springer-Verlag.

Dimarogonas, A.D., 1996. Vibration of cracked structures: a state of the art review. Engineering Fracture Mechanics 55, 831–857.

Doebling, S.W., Farrar, C.R., Prime, M.B., 1998. A summary review of vibration-based damage identification methods. Shock and Vibration Digest 30, 91–105.

Gasch, R., 1993. A survey of the dynamic behavior of a simple rotating shaft with a transverse crack. Journal of Sound and Vibration 160, 313–323.

Gross, T.S., Mendelsohn, D.A., 1988. On the effect of crack surface contact and friction due to fracture surface roughness in edge cracks subjected to external shear. Engineering Fracture Mechanics 31, 405–420.

Gross, T.S., Mendelsohn, D.A., 1989. Mode I stress intensity factors induced by fracture surface roughness under pure Mode III loading: Application to the effect of loading modes on stress corrosion crack growth. Metallurgical Transactions A 20A, 1989–1999.

Krawczuk, M., Ostachowicz, W., 1996. Damage indicators for diagnostic of fatigue cracks in structures by vibration measurements, a survey. Journal of Theoretical and Applied Mechanics 34, 307–326.

Nayeb-Hashemi, H., McClintock, F.A., 1982. Effects of friction and high torque on fatigue crack propagation in Mode III. Metallurgical Transactions A (Physical Metallurgy and Materials Science) 13 (12), 2197–2204.

Nayeb-Hashemi, H., Taslim, M.E., 1987. Effects of the transient Mode II on the steady state crack growth in Mode I. Engineering Fracture Mechanics 26, 789–807.

Nayeb-Hashemi, H., McClintock, F.A., Ritchie, R.O., 1983. Micro-mechanical modeling of Mode III fatigue crack growth in rotor steels. International Journal of Fracture 23 (3), 163–185.

Nayeb-Hashemi, H., Harrison, A., Vaziri, A., 2003. Dynamic response of a heat damaged fiber-resin beam subjected to harmonic forcing at the tip. Journal of Composites Technology and Research 25 (2), 87–95.

Panteliou, S.D., Chondros, T.G., Argyrakis, V.C., Dimarogonas, A.D., 2001. Damping factor as an indicator of crack severity. Journal of Sound and Vibration 241 (2), 235–245.

Panteliou, S.D., Dimarogonas, A.D., 1997. Thermodynamic damping in porous materials with ellipsoidal cavities. Journal of Sound and Vibration 201 (5), 555–565.

Rao, S.S., 2004. Mechanical Vibration. Prentice Hall.

Sekhar, A.S., Prabhu, B.S., 1994. Transient analysis of a cracked rotor passing through critical speed. Journal of Sound and Vibration 173, 415–421.

Tada, H., Paris, P.C., Irwin, G.R., 2000. The Stress Analysis of Crack Handbook, third ed. ASME Press.

Vaziri, A., Nayeb-Hashemi, H., 2002. Effects of local energy loss on the dynamic response of a cylindrical bar with a penny shape crack. IMECE 2002, New Orleans, LA.

Vaziri, A., Nayeb-Hashemi, H., 2003. Effective stress intensity factor in Mode III crack growth in round shafts. IMECE2003, Washington, DC.

Vaziri, A., Nayeb-Hashemi, H., 2005. The effect of crack surface interaction on Mode III crack growth in round shafts. Engineering Fracture Mechanics 72 (4), 617–629.

Vaziri, A., Nayeb-Hashemi, H. Dynamic response of a viscoelastic cylindrical bar with a penny shape crack under a harmonic axial load. International Journal of Mechanical Sciences, submitted for publication.